ChemComm

Accepted Manuscript

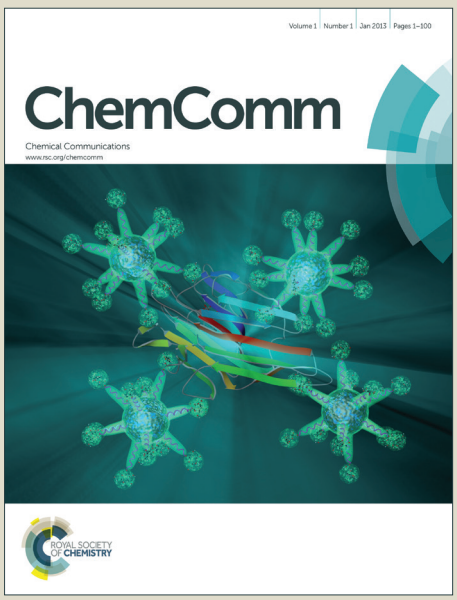

ROYAL SOCIETY OF CHEMISTRY

www.rsc.org/chemcomm

ChemComm

COMMUNICATION

N-doped nanodots/np$^+$-Si photocathodes for efficient photoelectrochemical hydrogen generation

Received 00th January 20xx,
Accepted 00th January 20xx

DOI: 10.1039/x0xx00000x

www.rsc.org/chemcomm

Deliang Chen,[a] Song Dai,[a] Xiaodong Su,[a] Yu Xin,[a] Shuai Zou,[a] Xusheng Wang,[a] Zhenhui Kang[b] and Mingrong Shen*[a]

Carbon nanodot treated by N_2-plasma is an effective catalyst for solar-driven hydrogen-evolved-reaction on np$^+$-Si photocathode and a support for Pt allowing for a reduction in Pt loading by a factor of about 3.5 while improving photoelectrochemical activity.

Photoelectrochemical (PEC) water splitting that converts intermittent solar radiation into hydrogen fuel is a potential processing route to solve the energy problem since hydrogen can be captured and utilized as a clean burning fuel or chemical feedstock.[1,2] Si is an promising material for the photocathode in a PEC cell, since its conduction band edge position is more negative than hydrogen evolution reaction potential for reduction of water to H_2.[3] However, the sluggish surface reaction is a major drawback for silicon. The noble metal platinum (Pt) is known as the most efficient and stable co-catalyst for hydrogen evolution. Unfortunately, Pt is an extremely scarce resource, making it expensive to use on a large scale for hydrogen production technologies. Thus, development of an efficient, low-cost and eco-friendly material as an alternative to noble metals is extremely important.[4,5]

Carbon nanodots (CNDs) are generally defined as small carbon nanoparticles with excellent properties such as chemical stability, nontoxity and easier large-scale production with low cost. CNDs have been coupled with semiconductor nanoparticles such as TiO_2, Ag_3PO_4, Fe_2O_3 and C_3N_4 to improve their photocatalytic abilities.[6-10] In addition, it was revealed that N is an excellent element for the stable chemical doping of carbon nanostructures such as carbon nanotubes and graphene to improve their photoelectron related properties, especially on the photocatalysis fields.[11,12] Recently, Sim et al. reported that monolayer graphene deposited onto a planar and microwire Si electrodes acts as an efficient hydrogen evolved reaction (HER) electrocatalyst and that N_2-plasma treatment enhances their catalytic activity.[13,14] The on-set potentials and the saturated photocurrents were (0.13 V vs. RHE, 32 mA/cm^2) and (0.26 V vs. RHE, 35 mA/cm^2) for the N-doped graphene-decorated planar and microwire Si photocathodes, respectively. However, they are still lower than the values for Pt decorated Si photocathodes,[15,16] indicating that carbon nanostructures may not be sufficient to replace Pt entirely. Recently, CNDs are used to enhance the PEC hydrogen generation of TiO_2 nanotube arrays, $SrTiO_3$ films and $BiVO_4$ inverse opals.[17-19] We are unaware of any published results for CNDs and/or N-doped CNDs (N-CNDs) as electro-catalysts on silicon photocathodes for HER. Comparing with monolayer graphene, CNDs are easier to produce with large-scale and low-cost. In this work we present the PEC results for np$^+$-Si photocathodes catalyzed by CNDs. Similar to monolayer graphene, the catalytic activity of CNDs can be boosted obviously by plasma treatment in N_2-ambient. In addition, we show that N-CNDs can be used as a support for Pt allowing for a reduction in Pt loading for HER.

The photocathode is constructed on single-crystal n-type silicon. An aluminum (Al)-doped p-type rear emitter is formed using a simple screen-printing process. On the front surface, the Si surface is protected by a 2nm thin Al_2O_3 layer.[20] We defined this as an np$^+$-Si photocathode. The CNDs are synthesized using an electrochemical ablation of graphite,[7] which are dispersed in water with concentration about 20 μg/mL. To produce CNDs/np$^+$-Si photocathode, 0.1 mL CND-contained water is dropped on the 1.3cm × 1.3cm Si electrode surface and then dried in the air under room temperature. Such deposition attaches about 1.2 μg/cm^2 CNDs on the Si surface. The PEC properties of the CNDs/np$^+$-Si photocathode can be optimized by changing the deposition times. The N_2-plasma treatment is performed using a capacitive coupled radio-frequency (27.12 MHz) discharge with a power of 100W, working pressure of 15Pa and time period of about 2 minutes.

[a] .College of Physics, Optoelectronics and Energy, Collaborative Innovation Center of Suzhou Nano Science and Technology, Photovoltaic Research Institute of Soochow University & Canadian Solar Inc., and Jiangsu Key Laboratory of Thin Films, Soochow University, Suzhou 215006, China. Email: mrshen@ suda.edu.cn
[b] Institute of Functional Nano & Soft Materials (FUNSOM), Jiangsu Key Laboratory for Carbon-based Functional Materials and Devices, and Collaborative Innovation Center of Suzhou Nano Science and Technology, Soochow University, Suzhou 215006, China

†Electronic Supplementary Information (ESI) available: Other information for the photoelectrodes (S1-S5).. See DOI: 10.1039/x0xx00000x

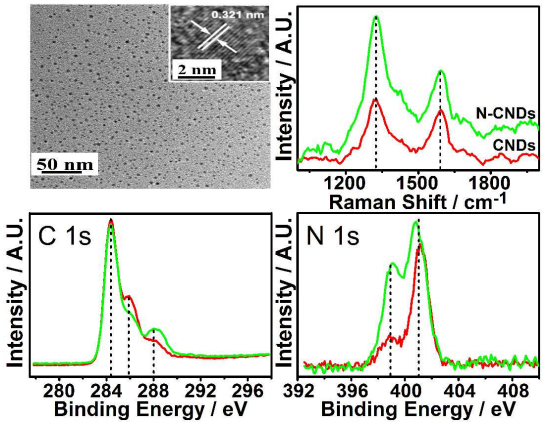

Fig. 1 (a) TEM images of the CNDs. Raman (b) and high-resolution XPS C1s (c) and N1s (d) spectra of the CNDs deposited on np^+-Si electrodes without and with N_2-plasma treatment.

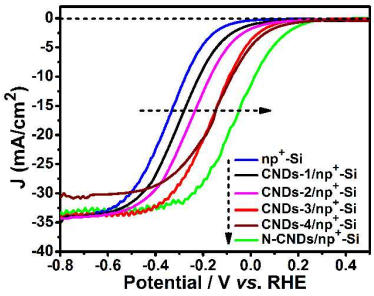

Fig. 2 *J-V* curves for np^+-Si photocathodes with and without CNDs deposited on the surface, using a scan rate of 25 mV/s and white light intensity of 100 mW/cm^2 Xe-lamp illumination.

Fig. 1a shows the transmission electron microscopy (TEM) image of the CNDs. They are spherical and fairly mono-dispersed, with diameters distributed in the range of 2 to 8 nm. High-resolution TEM in the inset of Fig. 1a shows that the lattice spacing of CNDs is 0.321 nm, in good agreement with the crystallographic <002> spacing of carbon.[21] The Raman spectrum of the CNDs shows both a G band at 1590 cm^{-1} due to in-plane vibration of sp^2 single-crystal graphite and a D band at 1320 cm^{-1} due to the presence of sp^3 disordered graphite (Fig. 1b). The obvious band in the D frequency region reflects a large disorder of bond angles, which can be good active sites for hydrogen production.[13] The relative intensity of the "disorder" D-band and the crystalline G-band (I_D/I_G) for as-produced CNDs is around 0.52. After the N_2 treatment, D-band becomes more evident, and I_D/I_G increases to 0.63, indicating the formation of abundant edges and defective sites in CNDs.

Fig. 1c,d illustrates x-ray photoelectron spectroscopy (XPS) results for C1s and N1s signal. In Fig. 1c, the peak at 284.4 eV can be identified as originating from C-C sp^2 structure. The higher energy peaks at 286.0 eV and 287.9 eV corresponding to sp^2 bonded C1s-N structure and sp^3 bonded C1s-N structure, respectively. The corresponding N1s-C binding energies are at 398.7 eV and 400.9 eV (shown in Fig. 1d), which confirm the presence of these two different bonding states between carbon and nitrogen.[22] After the N_2 treatment, both the sp^3 C1s-N and N1s-C XPS becomes more evident than the sp^2 peaks, manifesting that larger part of the N doping in present CNDs replace the carbon on the disordered sp^3 bond. As pointed out by Sim *et al.*,[13] abundant disordered bonds in the graphitic carbon could be catalytic sites for the HER, therefore, enhanced catalytic effect of CNDs after N_2 treatment is expected in this study.

The PEC characterization is carried out using a potentiostat (CH Instruments, CHI660E) in a three-electrode configuration. The measurements are conducted in an aqueous 1M perchloric acid solution (pH=0), using the photocathode as working electrode, a Ag/AgCl (3M KCl) as reference electrode and a Pt wire as the counter electrode. Fig. 2 shows a photocurrent density (*J*) *vs*. potential (*V*) scan for np^+-Si photocathodes with different amount of CNDs deposited on the surface under white light illumination. For the bare Si electrode without the decoration of CNDs, its photocurrent density increases gradually from about 0 V *vs*. RHE and is saturated at approximately 34 mA/cm^2 below -0.67 V *vs*. RHE. As expected, the overall *J-V* curves for the CND decorated electrodes are right-shifted obviously. If it is defined as the potential at the photocurrent density of 1mA/cm^2, the onset potential of the pristine Si photocathode is -0.08 V *vs*. RHE, and this potential is positively shifted to 0.11 V *vs*. RHE after the loading of CNDs by three-times, which corresponds to 3.6 μg/cm^2 CNDs presented on the electrode surface. This result indicates that CNDs can act as an effective catalyst for HER on the Si photocathode. However, one more time loading of the CNDs makes the saturated photocurrent decrease to 31 mA/cm^2. Note CNDs can absorb lots of visible light and the optical transmission at 600 nm of CNDs drop from about 90% to 55% with increasing CND loadings (Fig. S1, ESI †), but the saturated photocurrent densities of the corresponding CNDs/np^+-Si photocathodes in Fig. 2 barely change. It was reported CND itself can drive photocatalytic HER, and can form Z-scheme with other semiconductor like WO_3 to improve the HER.[23,24] Present studied indicates again that CNDs can contribute to the photocatalytic HER. However, further increased amount of the CNDs at the top of Si electrode causes less light absorption by Si, which diminish the synergistic light-to-photocurrent ability of the photocathode. Therefore, the optimal amount of CNDs on the electrode surface is 3.6 μg/cm^2. Such sample exhibits good stability during PEC measurements (Fig. S2, ESI †). This sample is then treated in the N_2-plasma. Fig. 2 also shows the *J-V* curve for the N-CND decorated np^+-Si photocathode. Compared with the one for CNDs/np^+-Si, the onset potential further right-shifts to 0.21V *vs*. RHE. As a result, the photocurrent at 0V *vs*. RHE increases from 3.4 to 10.9 mA/cm^2, indicating much higher catalytic activity for HER of the N-CNDs than the untreated CNDs.

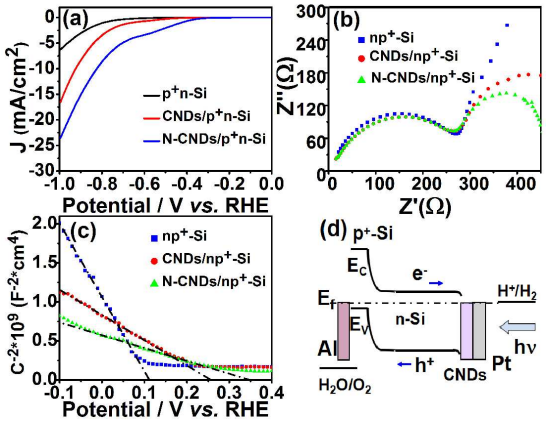

Fig. 3 (a) *J-V* scans under dark for the pure p$^+$n-Si, CNDs/p$^+$n-Si and N-CNDs/p$^+$n-Si electrodes respectively. Nyquist impedance plots (b) and Mott-Schottky plots (c) for the pure np$^+$-Si, CNDs/np$^+$-Si and N-CNDs/np$^+$-Si photocathodes. (d) The schematic band diagram of the CNDs/np$^+$-Si or N-CNDs/np$^+$-Si photocathodes.

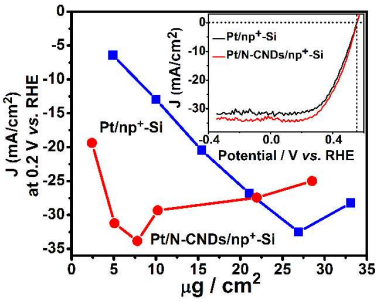

Fig. 4 The average photocurrent density at 0.2 V *vs*. RHE for the N-CNDs/np$^+$-Si and bare np$^+$-Si photocathodes following different amount of Pt loading. Inset: the *J-V* curves for the optimal energy conversion efficiency of the Pt/CNDs/np$^+$-Si and Pt/N-CNDs/np$^+$-Si photocathodes.

To further prove the catalytic activity for HER of both the CNDs and N-CNDs, they are coated on p$^+$n-Si electrodes respectively and the *J-V* scans under dark are performed to check their electrochemical performance. Note the p$^+$n-Si junction has a forward bias and low electrical resistance with negative potential *vs.* RHE in current case. Fig. 3a shows that the current density for CNDs coated p$^+$n-Si increases at a faster rate than that for pure p$^+$n-Si at potentials more negative than -0.4 V *vs*. RHE. After the surface is treated by the N_2 plasma, much faster rate is observed. At -1.0 V *vs*. RHE, the current density enhances from 6 mA/cm^2 for pure p$^+$n-Si, to 16 mA/cm^2 for CNDs/p$^+$n-Si, and to 23 mA/cm^2 for N-CNDs/p$^+$n-Si, manifesting the excellent electrocatalytic activity toward HER of the CNDs and N-CNDs.

We also performed electrochemical impedance spectroscopy (EIS) measurement to elucidate the charge-transfer resistances in different photocathodes. Two distinguishable semicircles in Fig. 3b can be observed in the Nyquist impedance plots. The left semicircle keeps nearly unchanged, while the second semicircle changes obviously, when the CNDs and N-CNDs are coated on the electrode surface. As discussed in our previous work, the second semicircle is governed by the charge separation and transfer at the front surface of electrode, whereas the left one is dominated by the rear np$^+$ junction.[20] The right semicircle for the CNDs and N-CNDs coated Si electrodes are dramatically smaller than that without CNDs, indicating much better improvement for the charge separation and transfer in the front Si surface region.

Fig. 3c shows the Mott-Schottky plots for the photocathodes. Capacitance measurements were performed as the potential was swept from -0.1 V to 0.4 V *vs*. RHE in a three-electrode cell without illumination. The flat band potential (E_{fb}) can be determined by extrapolation to a capacitance of zero.[14] The N-CNDs/np$^+$-Si electrode exhibits an E_{fb} of 0.35 V *vs*. RHE, whereas the E_{fb}s of the CNDs/np$^+$-Si and bare Si electrode are 0.26 V and 0.11 V *vs*. RHE, respectively. Higher band bending at the interface between the electrode and electrolyte promotes faster charge separation of photogenerated electrons and holes.[25] We also measured the open-circuit photovoltages (V_{ph}s) of the three samples (Fig. S3, ESI †). Upon illumination, the V_{ph}s of the N-CNDs/Si, CNDs/Si and the bare Si are 0.36, 0.26 and 0.10 V, respectively, consistent with the Mott–Schottky measurements.

The device structure of this work is rather non-conventional: the p$^+$n junction locates at the rear surface and the front surface exposes n-Si/electrolyte interface which does not work for HER. If there is no CNDs and Al_2O_3 layer on the electrode surface, an opposite weak barrier on the n-Si/electrolyte interface to that on the np$^+$ junction may form. As studied in our previous work, the height of this barrier can be lowered significantly after the coating of Al_2O_3 layer, resulting in the enhancement of the majority tunneling current.[20] In addition, CNDs have a work function of about 4.2 eV,[26] which is smaller than that ~4.4eV of Si. Therefore, we assume that a buried junction at CND/Al_2O_3/n-Si forms instead of n-Si/electrolyte interface at the front surface, which is favorable for the PEC reaction. Consequently, a band diagram of the electrolyte/CNDs/np$^+$-Si is schematically drawn in Fig. 3d. The E_{fb} for the CNDs or N-CNDs/np$^+$-Si photocathode can be enhanced due to the elimination of the opposite barrier.

As mentioned in the introduction, Pt is more active than carbon nanostructure for HER. Our previous study also showed that the Pt loaded np$^+$-Si photocathode has an on-set potential of 0.52V *vs*. RHE.[20] To check whether the N-CNDs are an effective support for Pt nanoparticles allowing for a reduction in Pt loading, we measured and compared the *J-V* curves for the N-CNDs/np$^+$-Si and bare np$^+$-Si photocathodes deposited with different amount of Pt catalyst through controlling the time during the electrochemical deposition. Note that we can get the exact Pt amount on the electrode surface based on the

current and time during electrochemical deposition (Fig. S4, ESI †). Fig. 4 shows that the on-set potential for N-CNDs/np^+-Si electrode reaches the maximum as the Pt amount is 7.8 μg/cm^2, while that for bare np^+-Si is 26.9 μg/cm^2. In Fig. 4, we draw the dependence of photocurrent density on the Pt amount taken from Fig. S4. The trends are the same with those of the on-set potential, etc., maximum photocurrent density at 7.8 μg/cm^2 for N-CNDs/np^+-Si and 26.9 μg/cm^2 for bare np^+-Si. The inset of Fig. 4 also shows that the saturated photocurrent density for N-CNDs/np^+-Si is higher than that for bare np+-Si (34.7 *vs*. 31.8 mA/cm^2), since more Pt on the surface of bare np^+ electrode will block more light to get into silicon. To qualitatively compare the amount of Pt deposited on the Pt(7.8 μg/cm^2)/N-CNDs/np^+-Si and Pt(26.9 μg/cm^2)/np^+-Si photocathodes we imaged them by SEM (Fig. S6, ESI †). Clearly there is more Pt on the latter photocathodes. Collectively, the PEC results and SEM images demonstrate that depositing a small amount (3.6 μg/cm^2) of N-CNDs onto np^+-Si is an effective means of reducing the required Pt loading by a factor of about 3.5 while improving PEC activity for the HER.

In summary, CNDs are demonstrated to be an effective catalyst for solar-driven HER on np^+-Si photocathodes and their catalytic activity can be boosted obviously by N_2-plasma treatment. The onset potential can be improved from -0.08 V *vs*. RHE for the bare np^+-Si photocathode, to 0.11 V *vs*. RHE for CNDs/np^+-Si, and further to 0.21V *vs*. RHE for N-CNDs/np^+-Si. XPS and Raman results revealed that the plasma treatment induced obvious sp^3 disorder C-C and C-N structures in the CNDs, which can act as catalytic sites, leading to better carrier transfer, electrochemical activity and higher E_{fb} on the electrode/electrolyte interface. In addition, N-CNDs can be used as a support for Pt allowing for a reduction in Pt loading by a factor of above 3.5 while improving activity for HER.

This work was supported by National Natural Science Foundation of China (Grant No. 91233109), Specialized Research Fund for the Doctoral Program of Higher Education (20133201110003), Natural Science Foundation of Jiangsu Education committee of China (15KJA140003) and a Project Funded by the Priority Academic Program Development of Jiangsu Higher Education Institutions (PAPD).

Notes and references

1 A. J. Bard and M. A. Fox, Acc. *Chem. Res.*, 1995, **28**, 141.
2 M. G. Walter, E. L. Warren, J. R. McKone, S. W. Boettcher, Q. X. Mi, E. A. Santori and N. S. Lewis, *Chem. Rev.*, 2010, **110**, 6446 .
3 R. N. Dominey, N. S. Lewis, J. A. Bruce, D. C. Bookbinder and M. S. Wrighton, *J. Am. Chem. Soc*., 1982, **104**, 467.
4 M. J. Kenney, M. Gong, Y. Li, J. Z. Wu, J. Feng, M. Lanza and H. Dai, *Science*, 2013, **342**, 836.
5 S. Hu, M. R. Shaner, J. A. Beardslee, M. Lichterman, B. S. Brunschwig and N. S. Lewis, *Science*, 2014, **344**, 1005.
6 H. T. Li, X. D. He, Z. H. Kang, H. Huang, Y. Liu, J. L. Liu, S. Y. Lian, C. H. A. Tsang, X. B. Yang and S. T. Lee, *Angew. Chem. Int. Ed.*, 2010, **49**, 4430.
7 H. C. Zhang, H. Ming, S. Y. Lian, H. Huang, H. T. Li, L. L. Zhang, Y. Liu, Z. H. Kang and S. T. Lee, *Dalton Trans.*, 2011, **40**, 10822.
8 H. Ming, Z. Ma, Y. Liu, K. M. Pan, H. Yu, F. Wang and Z. H. Kang, *Dalton Trans.*, 2012, **41**, 9526.
9 H. C. Zhang, H. Huang, H. Ming, H. T. Li, L. L. Zhang, Y. Liu and Z. H. Kang, *J. Mater. Chem.*, 2012, **22**, 10501.
10 J. Liu, Y. Liu, N. Y. Liu, Y. Z. Han, X. Zhang, H. Huang, Y. Lifshitz, S. T. Lee, J. Zhong and Z. H. Kang, *Science*, 2015, **347**, 970.
11 Z. H. Kang, E. B. Wang, B. D. Mao, Z. M. Su, L. Gao, S. Y. Lian and L. Xu, *J. Am. Chem. Soc.*, 2005, **127**, 6534.
12 W. J. Lee, J. M. Lee, S. T. Kochuveedu, T. H. Han, H. Y. Jeong, M. Park, J. M. Yun, J. Kwon, K. No, D. H. Kim and S. O. Kim, *ACS Nano*, 2012, **6**, 935.
13 U. Sim, T.-Y. Yang, J. Moon, J. An, J. Hwang, J.-H. Seo, J. Lee, K. Y. Kim, J. Lee, S. Han, B. H. Hong and K. T. Nam, *Energy Environ. Sci.*, 2013, **6**, 3658.
14 U. Sim, J. Moon, J. An, J. H. Kang, S. E. Jerng, J. Moon, S.-P. Cho, B. H. Hong and K. T. Nam, *Energy Environ. Sci.*, 2015, **8**, 1329.
15 I. Oh, J. Kye and S. Hwang, *Nano Lett.*, 2012, **12**, 298.
16 U. Sim, H.-Y. Jeong, T. Y. Yang and K. T. Nam, *J. Mater. Chem. A*, 2013, **1**, 5414.
17 F. Wang, Y. Liu, Z. Ma, H. T. Li, Z. H. Kang and M. R. Shen, *New J. Chem.*, 2013, **37**, 290.
18 X. Zhang, F. Wang, H. Huang, H. T. Li, X. Han, Y. Liu and Z. H. Kang, *Nanoscale*, 2013, **5**, 2274.
19 F. Nan, Z. H. Kang, J. L. Wang, M. R. Shen and L. Fang, *Appl. Phys. Lett.*, 2015, **106**, 153901.
20 R. L. Fan, J. W. Min, Y. A. Li, X. D. Su, S. Zou, X. S. Wang and M. R. Shen, *Appl. Phys. Lett.*, 2015, **106**, 213901.
21 H. T. Li, R. H. Liu, W. Q. Kong, J. Liu, Y. Liu, L. Zhou, X. Zhang, S. T. Lee and Z. H. Kang, *Nanoscale*, 2014, **6**, 867.
22 D. Marton, K. J. Boyd, A. H. Al-Bayati, S. S. Todorov and J. W. Rabalais, *Phys. Rev. Lett.*, 1994, **73**, 118.
23 P. Yang, J. H.Zhao, J.Wang, B.Y.Cao, L. Li and Z. P. Zhu, J. Mater. Chem. A, Doi: 10.1039/c5ta00657a.
24 X. M. Li, M. C. Rui, J. Z. Song, Z. H. Shen and H. B. Zeng, Adv. Funct. Mater. Doi: 10.1002/adfm. 201501250.
25 N. S. Lewis, *J. Electrochem. Soc.*, 1984, **131**, 2496.
26 Y. Li, Y. He, Y. Zhao, G. Q. Si, L. Deng, Y. B. Hou and L. T. Qu, *Adv. Mater.*, 2011, **23**, 776.